Breakup and Fusion of Self-Guided Femtosecond Light Pulses in Air

S. Tzortzakis,[1] L. Bergé,[2] A. Couairon,[2] M. Franco,[1] B. Prade,[1] and A. Mysyrowicz[1]
[1]*Laboratoire d'Optique Appliquée, ENSTA-École Polytechnique, Chemin de la Hunière, 91761 Palaiseau cedex, France*
[2]*Commissariat à l'Energie Atomique, CEA/DAM–Ile de France, B.P. 12, 91680 Bruyères-le-Châtel, France*
(Received 13 June 2000)

We report experiments showing the breakup and the merging of filaments formed by the modulational instability of femtosecond optical pulses in air. For input powers as high as 25 times the self-focusing threshold, the beams are shown to split into two spots, which coalesce into a self-guided beam. This effect occurs in an optically Kerr regime and plays an important role in the guiding process. Numerical simulations and theoretical estimates both support the comparison with the experimental data.

DOI: 10.1103/PhysRevLett.86.5470 PACS numbers: 42.65.Sf, 42.25.Bs, 42.65.Jx, 42.68.Ay

Nowadays, there is a considerable interest in understanding the propagation of femtosecond optical pulses through the atmosphere, in view of potential LIDAR applications [1]. Laser beams with high peak power are, indeed, known to form robust light guides over very long distances [2–4]. Various attempts in modeling this phenomenon have been proposed, by solving nonlinear Schrödinger-like systems [5–9]. Basically, an input beam having a transverse power, P_{in}, far above the threshold power for self-focusing, P_{cr}, first undergoes a compression in the diffraction plane caused by the Kerr response of air. Next, as its intensity increases by self-focusing, the beam ionizes the medium and creates an electron plasma. For subpicosecond infrared pulses with input intensities less than 10^{14} W/cm^2, optically induced ionization dominates through multiphoton processes [10]. The plasma then counteracts the optical self-focusing by digging a narrow hole in the radial wave profile [5] and by distorting the temporal shape of the beam [6,7,9]. From this dynamical balance between Kerr focusing and plasma defocusing, a self-guided light channel with a characteristic conical emission results [3–5].

However, issues still remain open about the inner dynamics of intense pulses in air. As is well known, a physical beam always exhibits small inhomogeneities that produce short-scale filaments in Kerr media via the modulational instability [11]. It was recently proposed in this respect [8] that under strong perturbations a broad beam with rather large waist ($w_0 \sim 0.7$ cm) and high power ($P_{\text{in}} \sim 35P_{\text{cr}}$) could propagate with a high density of collapsing filaments, regenerated by an accompanying background reservoir of low-amplitude energy. The light beam then forms an optically turbulent guide from multiple, recurrently nucleated filaments, which could maintain a long propagation. Besides, it was shown in [9] that for pulses with powers about $10P_{\text{cr}}$, the beam would produce only a finite number of filaments (mainly two spiky structures), which coalesce around the region of self-focus. On these points, clear observations are missing.

In this Letter, we study the propagation of femtosecond infrared beams exhibiting initially a single hump, with peak powers below 25 times critical. Emphasis is laid on two specific concerns. First, we examine the global features in the propagation and underline its three characteristic stages, namely, (i) the wave self-focusing (SF) in Kerr regime, (ii) the generation of an electron plasma by multiphoton ionization (MPI) and the formation of a self-guided beam, and (iii) the final spreading of the wave. These data, collected experimentally, are compared with results from a numerical code, which involves the main ingredients for describing the dynamics of ultrashort pulses in air. Second, we detail the early propagation of high-power beams. For different input powers, we investigate, both experimentally and theoretically, the breakup of beams with 3 mm waist and display evidence of their ability to merge into a single light guide. The onset of small-scale filamentation preceding the ionization is here thoroughly investigated. For clarity, the beam distortions caused by modulational instability will refer to "Kerr filamentation"; the "filament" resulting from MPI will be termed as light channel.

To start with, we identify the main stages in the dynamics of light self-guiding. From the experimental point of view, the laser source is a kHz, Ti:sapphire oscillator amplifier operating at the wavelength $\lambda_0 = 810$ nm. It delivers horizontally polarized pulses of 50 fs FWHM duration with an energy of up to 8 mJ per pulse. The wave diameter is first reduced by an inverted telescope, then the pulse is launched through the atmosphere in the form of a converging beam with focal distance $f = 2$ m, or as a collimated beam with $f = +\infty$. To record the intensity profiles, we use a pickup plate of BK7 glass at 45° angle. For intensities less than 10^{13} W/cm^2 (i.e., outside the focal region), the plate surface is not optically damaged and, therefore, the reflected part of the beam is not distorted. The reflected beam is imaged with a high aperture ($f/5$) lens onto a CCD camera. The intensity profile of the self-guided pulse and the electron density resulting from air ionization are measured along the propagation axis for different input pulse energies, E_{in}, insured with a relative error of $\pm 10\%$. We also perform far-field measurements of the energy in the resulting light channel after isolating it with a pinhole. Electrons are detected by using the electric-conductivity

 0031-9007/01/86(24)/5470(4)$15.00

technique described in Ref. [12], with synchronous detection adapted to the high repetition rate of our laser system. As in our previous experiments, we measure air resistivity by recording the current flowing between two plane copper electrodes connected by the laser-induced plasma. We calibrate the current as a function of the electron density averaged over the measured beam diameter ~0.5 mm enclosing the light channel, by means of an optical technique probing the plasma decay [13]. The threshold sensitivity of our experimental technique corresponds to an average electron density of $\rho_{\rm th} \sim 10^{15}$ cm^{-3}, represented by the dotted line in Fig. 1.

Numerical simulations are carried out for comparison with these experiments. We employ a three-dimensional code constrained to the axial symmetry, whose basic scheme was detailed in [9]. It resolves the slowly varying envelope of the linearly polarized laser electric field $\mathcal{E}(r,z,t)$, with central wave number $k_0 = k(\omega_0)$ and amplitude expressed in $\sqrt{W}$/cm, which is governed by an extended nonlinear Schrödinger (NLS) equation in the frame moving with the pulse

$$2i\frac{\partial \mathcal{E}}{\partial z} + \frac{1}{k_0}\Delta_\perp \mathcal{E} - k''\frac{\partial^2 \mathcal{E}}{\partial t^2} + k_0 n_2\left\{|\mathcal{E}|^2 + \frac{1}{\tau_K}\int_{-\infty}^{t} e^{-(t-t')/\tau_K}|\mathcal{E}(t')|^2\,dt'\right\}\mathcal{E} - k_0\frac{\omega_{pe}^2(\rho)}{\omega_0^2}\mathcal{E} + i\beta^{(K)}|\mathcal{E}|^{2K-2}\mathcal{E} = 0, \quad (1)$$

coupled with the electron density ρ of plasma created by multiphoton transitions. This quantity evolves as

$$\frac{\partial \rho}{\partial t} = \frac{\beta^{(K)}}{K\hbar\omega_0}|\mathcal{E}|^{2K}\left(1 - \frac{\rho}{\rho_{at}}\right), \quad (2)$$

where $\rho_{at} = 2.7 \times 10^{19}$ cm^{-3} is the density of neutral atoms satisfying $\rho/\rho_{at} \leq 1\%$. In Eq. (1), z refers to the propagation distance, the two-dimensional Laplacian $\Delta_\perp$ describes the transverse diffraction, and the remaining terms are the group-velocity dispersion (GVD) with coefficient $k'' = 0.2$ fs^2/cm, the Kerr response of air, with both instantaneous and retarded components in ratio $\frac{1}{2}$ fixed by experimental evidence [14], the electron density entering the plasma frequency $\omega_{pe}^2(\rho) = q_e^2\rho/m_e\epsilon_0$ (q_e and m_e are the electron charge and mass), and multiphoton absorption (MPA) with coefficient $\beta^{(K)}$. At atmospheric pressure, the appropriate parameters are $n_2 = 3.2 \times 10^{-19}$ cm^2/W, $K = 10$ for a mean ionization potential $U_i = 14.6$ eV, $\beta^{(10)} \simeq 1.27 \times 10^{-126}$ cm^{17}/W^9 [10,15], $\tau_K = 70$ fs is the characteristic time of molecular motions of air, and the critical power for self-focusing is $P_{\rm cr} = \lambda_0^2/2\pi n_2 \simeq 3.3$ GW. The input beams are modeled by unperturbed Gaussians with power $P_{\rm in}$ [9]. They exhibit a transverse waist $w_0 = 3$ mm ($|\mathcal{E}| \sim e^{-r_\perp^2/w_0^2}$), a temporal FWHM diameter $\Delta T = 50$ fs, and they are either collimated ($f = +\infty$) or focused by a lens with focal length $f = 2$ m [6,9]. We have simulated the evolution of a focused beam with $E_{\rm in} = 5$ mJ and $f = 2$ m, which we compare with experiments performed at the same energy level ($P_{\rm in} \sim 25P_{\rm cr}$). In Fig. 1, we show the radius of the beam and the maximum-in-time electron density, averaged in the radial plane. Apart from discrepancies near the focal point, the numerical results are in good agreement with the experimental measurements. We retrieve the SF stage, followed by an ionization front that remains clamped with the pulse at intensities $\leq 10^{14}$ W/cm^2 and enables light channeling over ten Rayleigh lengths, $z_f = z_0 f^2/(z_0^2 + f^2) \sim 11.4$ cm. Here, $z_0 = \pi w_0^2/\lambda_0 \sim 35$ m is the diffraction length of the collimated beam. Thus, for powers $P_{\rm in}$ around $25P_{\rm cr}$ and narrow waists, the beam self-focuses, creates an electron plasma, and then forms a self-guided light channel with ~100 μm diameter over more than 1 m.

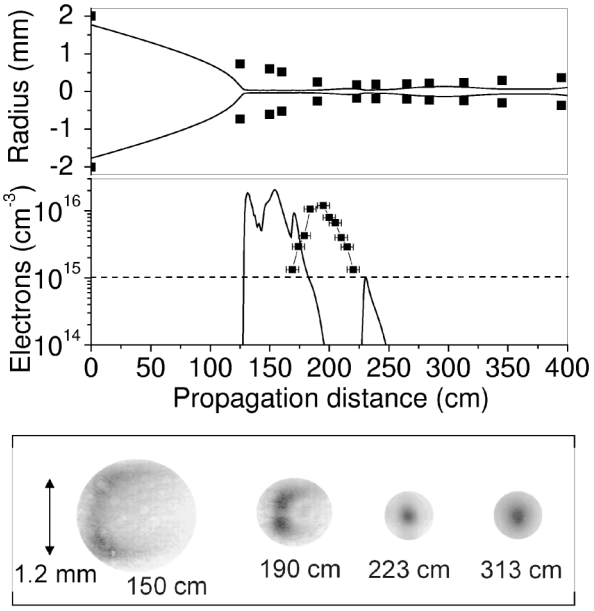

FIG. 1. Experimental results for the mean radius $R(z)$ of a focused beam with energy $E_{\rm in} = 5$ mJ and for the electron density ρ (squares). The numerical counterparts are shown in solid lines [$R(0) = w_0\sqrt{\ln 2/2}$]. The dotted line represents the electron detection threshold. Bottom inset: Dynamics of the 5 mJ beam profile at different propagation distances.

The energy captured in this channel is numerically found to be close to 10% of the input energy, which was confirmed by the experiment. The propagation length covering the early SF range, $z \leq z_c \simeq 1.4 \pm 0.1$ m, is about that attained by a collapsing beam in a purely Kerr medium with an instantaneous response only and an effective critical power $P'_{\rm cr} = 2P_{\rm cr}$. It can readily be determined by employing Marburger's formula [11]: $z_c = z_0/(\chi_M + z_0/f)$ with $\chi_M = (0.367)^{-1}[(\sqrt{P_{\rm in}/P'_{\rm cr}} - 0.852)^2 - 0.0219]^{1/2}$. The number for the maximum electron density is consistent with the simple estimate $\rho \sim \Delta T\beta^{(K)}I^K/K\hbar\omega_0$ that

varies as $(0.25-7.3) \times 10^{16}$ cm^{-3} in the intensity range $I = (5-7) \times 10^{13}$ W/cm^2 attained near focus.

The global features of femtosecond pulse propagation in air are, at least qualitatively, well described by the model equations (1) and (2). However, inspection of the beam profile around the location of the focus reveals a more complex structure. As shown in the inset of Fig. 1, the beam does not evolve as a single-hump Gaussian. Instead, it forms a spatial ring, which breaks up along the vertical axis in two symmetric spots that finally fuse into one central lobe. Ring and two-spot formation mainly results from the Kerr filamentation, which is triggered by small-scale inhomogeneities. In this regard, numerical simulations using the experimentally recorded beam profiles instead of unperturbed Gaussians reproduced the phase of ring formation. Although they did not restore the two-spot pattern because of the constraint imposed by the axial symmetry, these simulations showed amplification and merging of rings *before* the ionization front.

From now on, we examine this early filamentation stage. To make it more visible, we use beams in collimated geometry, which expands the region of interest by suppressing the space compression introduced by the lens. The results are detailed in Fig. 2. This figure shows transverse intensity patterns for input energies varying from 1 mJ ($P_{\rm in} \sim 5P_{\rm cr}$) to 5 mJ ($P_{\rm in} \sim 25P_{\rm cr}$). At low energies (1 mJ, top row), the first sequence illustrates the basic self-focusing, a short guiding, and the final spreading of the beam. At moderate energies (2.5 mJ, middle row), the beam begins to form a ring structure, which breaks up into two distinct spots. Both spots then coalesce in a single lobe that finally disperses at $z = 8.5$ m. At still higher energy (5 mJ, lower row), this scenario becomes clearly apparent. Being modulationally unstable, the beam first decays into an elliptical ring that gives rise to two spots [$z = 2.5-4.5$ m] with typical radial dimensions of the order $\sim$1.5 mm. Those self-focus at their own centroids, before fusing at larger distances [$z = 6.5-8.5$ m]. This evolution is thus generic.

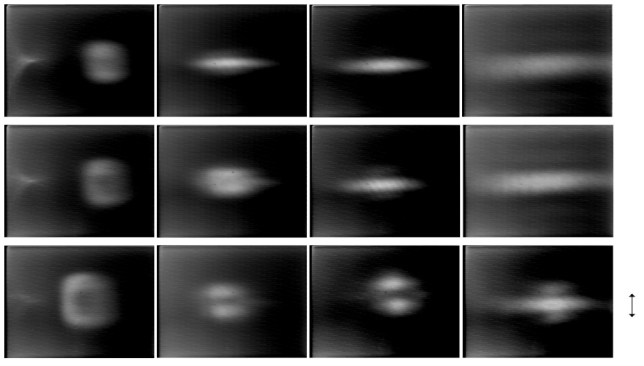

FIG. 2. Propagation patterns of 50 fs unfocused beams in air at different propagation distances = 2.5, 4.5, 6.5, and 8.5 m (for each row, from left to right). Top row: $E_{\rm in} = 1$ mJ; middle row: $E_{\rm in} = 2.5$ mJ; bottom row: $E_{\rm in} = 5$ mJ. The arrow on the right represents a length scale of 2 mm.

To explain this mechanism, we derive analytical estimates from a simplified nonlinear Schrödinger model. At leading order, we consider Eq. (1), in which the electron density is frozen in time and acts as a global saturating nonlinearity. Although strong temporal distortions are known to arise from MPI at high density levels, i.e., after the focus point z_c [6–9], such an approximation holds in the early range $z < z_c$, where the nonlinearities mainly originate from the Kerr term. We verified numerically that the pulse temporal profiles remained unchanged in this early propagation domain. The electron density is thus approximated by $\rho = \Delta T \beta^{(K)} |\mathcal{E}|^{2K}/(K\hbar\omega_0)$. Accordingly, we omit the delayed component in the Kerr response. This amounts to considering an effective critical power for self-focusing being twice $P_{\rm cr}$. We also ignore GVD and MPA, which never significantly affect the beam dynamics in this range, i.e., until far beyond the ionization threshold [8,9]. Therefore, we deal with the NLS equation

$$2ik_0 \frac{\partial \mathcal{E}}{\partial z} + \Delta_\perp \mathcal{E} + k_0^2 (n_2 |\mathcal{E}|^2 - n_{2K} |\mathcal{E}|^{2K}) \mathcal{E} = 0, \tag{3}$$

where $n_{2K} \simeq 1.3 \times 10^{-143}$ cm^{2K}/W^K. Following the Bespalov-Talanov procedure (see, e.g., [11]), we first determine the incidence of perturbations in the form $\delta\mathcal{E} \sim e^{\gamma z + i\vec{k}_\perp \cdot \vec{r}_\perp}$ with growth rate γ and transverse wave number $k_\perp$, which develop on the beam having the uniform averaged intensity $I_0 = |\mathcal{E}_0|^2$ ($\delta\mathcal{E} \ll \mathcal{E}_0$). The growth rate provides the transverse spacing between filaments, $\Lambda_\perp = [2\pi P_{\rm cr}/I_0(1 - \alpha I_0^{K-1})]^{1/2}$, and their growth length $\Lambda_z \sim \gamma_{\rm max}^{-1} = \Lambda_\perp^2/\pi^2\lambda_0$, where $\alpha \equiv K n_{2K}/n_2$. From these, we infer that MPI efficiently counteracts the Kerr focusing for $I_0 \geq \alpha^{1/(1-K)} \sim 5 \times 10^{13}$ W/cm^2. At moderate intensity levels, $I_0 \leq 10^{13}$ W/cm^2, the dynamics is thus essentially driven by the Kerr response of the medium. For an input intensity of $I_0 = E_{\rm in}/\langle S \rangle \Delta T \simeq (0.7-1) \times 10^{12}$ W/cm^2 with $E_{\rm in} = 5$ mJ distributed on the average surface $\langle S \rangle = \pi w_0^2/2$, we find that filaments form over distances $\Lambda_z \geq 1.2$ m with a transverse size $\Lambda_\perp \simeq 1.8$ mm. These estimates are compatible with the filament growth length and spot sizes detailed in Fig. 3. The first filamentation mode is an annular ring, promoted by almost isotropic perturbations. As this ring is still modulationally unstable with an extension of about 4.5 mm, two cells emerge from it, in agreement with the patterns of Fig. 2. Next, both spots increase in intensity: Using $E_{\rm spot} \simeq 2.5$ mJ and $\langle S \rangle \simeq \pi w_x w_y/2$ computed with the horizontal and vertical spot waists w_x, w_y, I_0 in each spot is found to reach the maximum value $I_0 \simeq 3 \times 10^{12}$ W/cm^2 at $z = 6.5$ m, before the two filaments merge. The wave intensity has thus increased by less than one decade. Because I_0 always remains below 10^{13} W/cm^2, MPI is of negligible influence and, indeed, no significant emission of electrons above $\rho_{\rm th}$ was detected with collimated beams, at least along distances accessible experimentally ($z < 10$ m).

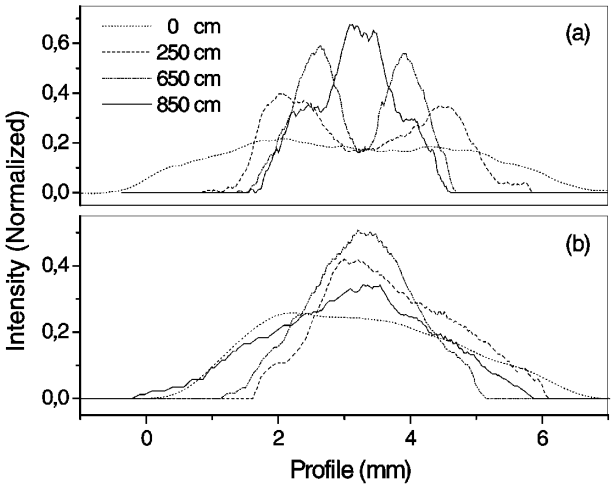

FIG. 3. Measured intensity profiles of a 5 mJ beam with $f = +\infty$ along (a) the y axis (vertical cut) and (b) the x axis (horizontal cut along one spot) at $z = 0$ (dotted line), $z = 2.5$ m (dashed), $z = 6.5$ m (dash-dotted), and $z = 8.5$ m (solid).

In contrast, the mean intensity of the convergent beam shown in Fig. 1 was found to exceed 5×10^{13} W/cm^2 around the linear focus.

As a result, the first propagation stage is actually driven by the Kerr response of air that focuses the beam and breaks it up through modulational instability into two filaments, which is well described by Eq. (3). Note that although each spot might in theory further split with a power $P_{\rm fil} \simeq \pi\Lambda_\perp^2 I_0/4 \approx \pi^2 P_{\rm cr}/2 < 12.5 P_{\rm cr}$ [9,11], only two local intensity maxima are clearly observed here.

Let us now discuss the mutual coalescence of spots, which, for simplicity, we model by two in-phase Gaussians arising at a given $z = z_0$, with waist w_α, individual power P_α, and mutual separation distance δ. We assume that the two spots are identical ($P_1 = P_2$), symmetrically located from the center of coordinates, and they possess equal sizes $\sim w_\alpha$ along the (x, y) directions. They are initially "well separated" with $\delta > \sqrt{2}\, w_\alpha$ [16], which is satisfied by the spots emerging at $z_0 = 6.5$ m in Fig. 3. In SF regime, coalescence results from the vanishing of the total mean-square radius of the beam, denoted by $\langle r_\perp^2 \rangle$, provided that both spots strongly interact. By neglecting MPI for collimated beams, this process can be described from the evolution equation, $d_z^2 \langle r_\perp^2 \rangle = H/k_0^2 P_\alpha$, where H is the Hamiltonian of Eq. (3) expressing at leading order as $H \simeq \int (|\nabla_\perp \mathcal{E}|^2 - \pi |\mathcal{E}|^4/P_{\rm cr})\, d\vec{r}_\perp = H_{\rm free} + H_{\rm int}(\delta)$. Here $H_{\rm free}$ refers to the Hamiltonian contributions of each individual spot and $H_{\rm int}(\delta)$ gathers all interaction terms that exponentially decrease with δ (see [16] for more detail). Self-focusing follows whenever $H < 0$, and the predominance of the interaction terms requires that δ be less than $3w_\alpha$ for P_α above critical. Thus, the two spots can fuse for $\delta < 3w_\alpha$, which definitely applies to the separation distance measured in Fig. 3 at $z = 6.5$ m. It is worth noticing that, in the absence of wave collapse, the fusion is all the more delayed along z as the spots are intense, since at increasing energy they reinforce their own local attractor on their individual centroids. This effect contributes to enlarge the Kerr stage beyond which an electron plasma can be excited, as confirmed by Fig. 2. For a focused beam, $\langle r_\perp^2 \rangle$ vanishes faster (see, e.g., [9]), and the fusion dynamics is accelerated.

In conclusion, we have shown that the early stages preceding the self-guiding in air of femtosecond pulses with peak power lying between 5 and 25 $P_{\rm cr}$ consisted in the breakup of the beam into two spots by modulation instability and their coalescence into one central lobe. This process gives rise to self-channeled light guides. The main stages in the formation of light channels have been confronted with numerical simulations restoring the different propagation regimes inherent to the self-focusing, plasma formation, self-guiding, and ultimate dispersion of the beam. In addition, by means of the NLS model (3), we have justified the filament formation and the fusion process enabling the beam to recombine into one robust lobe. This scenario of breakup and coalescence preceding the self-guiding is *generic, both for focused and for unfocused beams*, in the domain of powers investigated. Note that this does not prevent higher-power pulses to decay into more filaments, as proposed in [8]. To the best of our knowledge, we provided, for the first time, clear evidence of optical coalescence following the filamentation of femtosecond lasers in air, and we obtained good agreements between experimental data, numerical results, and recent theories in this field.

The authors thank Y. B. André and G. Mullot for technical assistance, and A. Chiron, M. Kolesik, and E. Wright for fruitful discussions.

[1] L. Wöste *et al.,* Laser Optoelektron. **29**, 51 (1997).
[2] A. Braun, G. Korn, X. Liu, D. Du, J. Squier, and G. Mourou, Opt. Lett. **20**, 73 (1995).
[3] E. T. J. Nibbering *et al.,* Opt. Lett. **21**, 62 (1996).
[4] B. La Fontaine *et al.,* Phys. Plasmas **6**, 1615 (1999).
[5] V. P. Kandidov, O. G. Kosareva, and S. A. Shlenov, Quantum Electron. **24**, 905 (1994).
[6] M. Mlejnek, E. M. Wright, and J. V. Moloney, Opt. Lett. **23**, 5 (1998); J. Schwarz *et al.,* Opt. Commun. **180**, 383 (2000).
[7] A. Chiron *et al.,* Eur. Phys. J. D **6**, 383 (1999).
[8] M. Mlejnek, M. Kolesik, J. V. Moloney, and E. M. Wright, Phys. Rev. Lett. **83**, 2938 (1999).
[9] A. Couairon and L. Bergé, Phys. Plasmas **7**, 193 (2000); L. Bergé and A. Couairon, Phys. Plasmas **7**, 210 (2000).
[10] L. V. Keldysh, Sov. Phys. JETP **20**, 1307 (1965).
[11] J. H. Marburger, Prog. Quantum Electron. **4**, 35 (1975).
[12] S. Tzortzakis *et al.,* Phys. Rev. E **60**, R3505 (1999).
[13] S. Tzortzakis *et al.,* Opt. Commun. **181**, 123 (2000).
[14] J. F. Ripoche *et al.,* Opt. Commun. **135**, 310 (1997).
[15] A. Talebpour, J. Yang, and S. L. Chin, Opt. Commun. **163**, 29 (1999).
[16] L. Bergé *et al.,* J. Opt. Soc. Am. B **14**, 2550 (1997).